XRD, XPS and ^{119}Sn NMR study of tin sulfides obtained by using chemical vapor transport methods

M. Cruz,[a] J. Morales,[a,*] J.P. Espinos,[b] and J. Sanz[c]

[a] *Departamento de Química Inorgánica e Ingeniería Química, Facultad de Ciencias, Edificio C3, Campus de Rabanales, Universidad de Córdoba, E-14004 Córdoba, Spain*
[b] *Instituto de Ciencias de Materiales de Sevilla, Avda. Américo Vespucio s/n, Sevilla, Spain*
[c] *Instituto de Ciencias de Materiales de Madrid, Cantoblanco, Madrid, Spain*

Abstract

Application of the chemical vapor transport method to the Sn–S system allowed three different phases (viz. SnS, SnS_2 and Sn_2S_3) to be synthesized. No evidence of the formation of other, previously reported mixed valence compounds such as Sn_3S_4 or Sn_4S_5 was found, whichever the Sn:S atomic ratio and temperature gradient used. Except for SnS_2, which was always obtained as a pure phase as a result of starting from the required stoichiometry, a mixed phase was invariably obtained. The XPS spectrum for Sn_2S_3 was only slightly different from those for SnS and SnS_2 in spite of the presence of Sn(II) and Sn(IV) in the former compound, which hindered the identification of mixed valence compounds in the Sn–S system by the use of this spectroscopic technique. By contrast, the chemical shifts, anisotropy and skew parameters for Sn_2S_3 as obtained by ^{119}Sn NMR were markedly different from those for SnS and SnS_2, and reflected the severe distortion of Sn(IV) and, especially, Sn(II) in the former compound relative to the latter two. The time scale for this resonance technique is shorter than the lifetime of the valence states, which allows one to unambiguously distinguish the two oxidation states of Sn.

1. Introduction

At least three mixed valence compounds in the S–Sn system have been reported to date, namely: Sn_2S_3 [1], Sn_3S_4 [2] and Sn_4S_5 [3]. Only the former, however, has been characterized in structural terms, from X-ray single-crystal studies [4]. The characterization of the other two is somewhat less accurate and in, the case of Sn_3S_4, the information contained in the JCPDS card [5] is restricted to interplanar distances and peak intensities. These compounds behave as semiconductors, and are thus of potential interest as photovoltaic materials for use in efficient solar cells [6].

In the course of various studies on SnS_2 and SnS single crystals [7] we found needle-shaped crystals the structure of which matched that of Sn_2S_3 during their synthesis. This finding prompted us to re-examine the S–Sn system using high-temperature chemical vapor transport methods for synthetic purposes and X-ray powder diffraction (XRD), X-ray photoelectron spectroscopy (XPS) and [119]Sn nuclear magnetic resonance (NMR) for characterization.

2. Experimental

The tin sulfides were prepared from their constituent elements, namely: purified tin powder (Strem Chem.) and dry elemental sulfur (Merck). The starting mixtures, in the pellet form (7 mm diameter), were prepared from the individual elements in the required mole ratio and sealed in evacuated silica tubes 20 cm long × 1.6 cm i.d. The tubes were heated at 550°C for 2 days. Crystals from these samples were ground by hand, mixed with a small amount of I_2 used as the transport agent (ca. 5 mg/cm³) and re-sealed in evacuated silica tubes. The transport tubes were placed in a two-zone furnace where charge-growth gradients of 950–850°C, 850–750°C and

*Corresponding author. Fax: 34-957-218621.
E-mail address: iq1mopaj@uco.es (J. Morales).

750–650°C were used over a growth period of 10 days. Sealed tubes were opened in an Mbraun dry-box, and crystals washed several times with acetonitrile to remove iodine impurities and subsequently stored under an argon inert atmosphere for further characterization. Thus, contact of the sample with the atmosphere was restricted to the time needed for the crystals to be transferred to the measurement chamber of the spectrometers.

XRD patterns for the ground crystals were recorded on a Siemens D5000 diffractometer, using $CuK\alpha_{1,2}$ radiation and a graphite monochromator. The scan conditions were $15–110°$ (2θ), a $0.03°$ (2θ) step and 15 s per step. To avoid the reactivity of samples towards moisture, a piece of Mylar plastic was used to isolate the powder.

XPS experiments were performed on an ESCALAB 200 spectrometer operating in the constant pass energy mode (50 eV) and using unmonochromated $MgK\alpha$ radiation (1253.6 eV) as excitation source. The base pressure in the analysis chamber was $<10^{-9}$ mbar. A sputtered silver foil was used to evaluate experimental energy resolution. In this case, the full-width measured at half-maximum of the Ag $3d_{5/2}$ signal was 1.5 eV. Crystals were attached to a copper sample holder with the aid of conducting silver epoxy resin. Clean surfaces were obtained in the spectrometer preparation chamber by scraping with a steel blade. The binding energy reference for the S $2p$ core level was taken to be 161.7 eV, consistent with the value previously reported for S^{2-} in different layered sulfides [8].

^{119}Sn NMR spectra were obtained at room temperature on a MSL-400 Bruker spectrometer operating at 149.11 MHz. Magic angle spinning (MAS) NMR spectra were recorded upon irradiation of the sample with a $\pi/2$ pulse (4 μs). The rotor used was of the Andrew type and the spinning frequency 4 kHz. In order to reduce saturation effects, the time interval chosen between successive was 30 s. The number of scans was 200. The reference for the ^{119}Sn NMR spectra was a 5% solution of tetramethyltin in dichloromethane. NMR spectra were processed by using the software Winfit (Bruker). The spinning rate and positions, linewidths and intensities of the components were determined with a standard, non-linear least-squares fitting method; however, chemical shift anisotropies (anisotropy and asymmetry) are adaptable parameters so they must be determined by trial and error. For quantitative purposes, the sum of the integrated intensities of the spinning side bands corresponding to each component was determined.

3. Results and discussion

Table 1 shows the phases detected by X-ray diffraction for the three selected temperature gradients of growth and the five stoichiometric mixtures studied, which were chosen in terms of their tin sulfide stoichiometry as described earlier. Only at an Sn:S ratio of 1:2 was a single-phase SnS_2 2H type structure obtained, whatever the temperature range. With a unity Sn:S ratio, pure SnS was only obtained over the higher temperature range used (950–850°C). The remaining stoichiometries tended to yield a mixed phase with SnS and Sn_2S_3 as the dominant components (none led to a pure compound). The sole mixed valence compound obtained was Sn_2S_3. No other previously reported phases such as Sn_3S_4 and Sn_4S_5 were detected under the experimental conditions used in this study, even if an appropriate Sn:S atomic ratio was used. Nevertheless, because of the similarity of the patterns for Sn_3S_4 and Sn_2S_3, diffraction files 27-0900, 4-0619, respectively, Sn_2S_3 crystals were structurally characterized by Rietveld refinement of the XRD data [9], using the GSAS software suite [10]. The atomic positions used in the X-ray refinement of the compound were taken from Ref. [4] and the final structural parameters are summarized in Table 2; also, the difference between the observed and calculated diffraction profiles is shown in Fig. 1. The refinement in the orthorhombic symmetry converged on $a = 0.8869$ nm, $b = 0.3748$ nm $c = 1.4021$ nm, $R_{WP} = 10.23\%$ and $R_F = 2.88\%$. These values are in good agreement with the crystal structure derived from single-crystal X-ray diffraction data and reflect the high purity of the phase obtained.

For the spectroscopic studies, the crystals were picked out with tweezers. This task was made easier by the different crystal morphology of the three phases identified. Thus, Sn_2S_3 was obtained as needle-shaped

Table 1
Phases detected by X-ray diffraction analysis

Temperature (°C) Sn:S atomic ratio	950–850	850–750	750–650
1:1	SnS	$SnS + Sn_2S_3$	$Sn_2S_3 + SnS$
2:3	$Sn_2S_3 + SnS$ (traces)	$SnS + Sn_2S_3 + SnS_2$	$Sn_2S_3 + SnS$
3:4	$Sn_2S_3 + SnS$	$SnS + Sn_2S_3 + SnS_2$	$Sn_2S_3 + SnS$
4:5	$Sn_2S_3 + SnS$	$SnS + Sn_2S_3$	$Sn_2S_3 + SnS$ (traces)
1:2	SnS_2	SnS_2	SnS_2

Table 2
Positional and thermal ($\mathring{A}^2$) parameters for Sn_2S_3

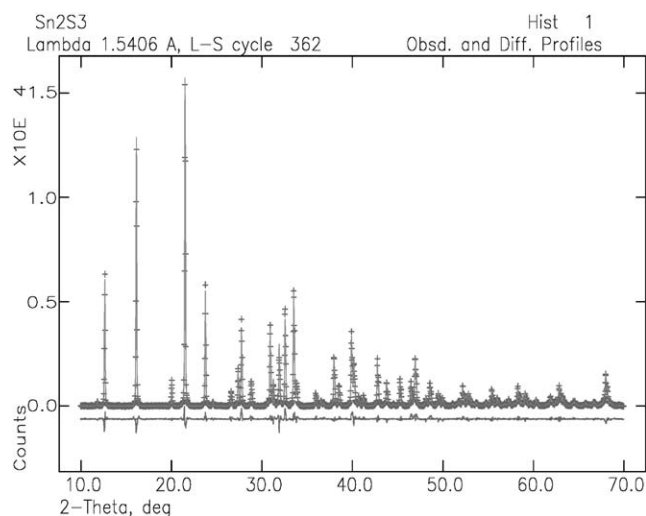| Atom	x	y	z	U_{iso}
Sn (1)	0.16575	0.25	0.05191	0.726
Sn (2)	0.48621	0.75	0.16997	1.133
S (1)	−0.01251	0.75	0.10881	0.600
S (2)	0.33761	0.75	−0.00589	0.583
S (3)	0.28511	0.25	0.21377	0.281

All atoms are located at the $4c$ position of the space group *Pnma*.

Fig. 1. Rietveld plot for Sn_2S_3 with orthorhombic *Pnma* structure.

Table 3
XPS elemental analysis (%) for SnS, Sn_2S_3 and SnS_2 samples

Peak	SnS	Sn_2S_3	SnS_2
I $3d_{5/2}$	—	5.0	—
O 1s	a	11.1	a
Sn $3d_{5/2}$	52.1	40.7	38.5
S $2p$	47.9	43.1	61.5
Sn/S atomic ratio	1.08	0.94	0.62

[a] Estimated to be below 2%.

crystals several millimetres long, whereas SnS_2 was obtained as golden plate-like crystals of variable size ranging from 1 to 5 mm in diameter and several tenths of a millimetre in thickness. The SnS phase was obtained as shiny black crystals of ill-defined morphology.

The XPS spectra revealed that the crystal surfaces of SnS and SnS_2 were highly clean and that they contained trace amounts ($<2\%$) of oxygen (see Table 3). The highest consistency between the experimental (1.08) and theoretical Sn/S atomic ratio was observed for SnS; for SnS_2, however, the experimental ratio exceeded that calculated from the nominal stoichiometry. Contamination in Sn_2S_3 crystals was somewhat greater. In addition to that for oxygen, the I $3d$ peak was detected (as a very

Table 4
Binding energies and Auger transition parameter of the main core-level spectra for tin sulfides (eV)

Compound	S $2p$	Sn $3d_{5/2}$	Sn_{LMM}	α^a Sn
SnS	161.7 (2.45)	486.0 (2.05)	435.4	921.4
Sn_2S_3	161.7 (2.47)	486.6 (2.22)	434.1	920.7
SnS_2	161.7 (2.40)	486.5 (2.00)	434.3	920.8

[a] Wagner–Auger parameter values are also shown. Values in parentheses: full-widths at half-maximum.

weak signal). Attempts at finding crystals containing no iodine failed. Also, an attempt at obtaining this phase from a stoichiometric mixture of Sn and S without I_2 as transport agent failed. For this reason all subsequent comments refer to the crystals the composition of which is shown in Table 3. If one assumes that oxygen and iodine are as SnO_2 and SnI_4, respectively, then more than 80% of Sn should be bound to S. As a result, the binding energy measurements must essentially describe the Sn–S interactions. The calculated value for the Sn/S ratio would be ca. 0.75 and higher than that derived from stoichiometric considerations, which is similar to that found for SnS_2. Strictly, this would mean that the surface composition of both compounds contains excess Sn. Oxygen contamination as the origin of this anomaly is unlikely. In fact, the oxygen contents in Table 3 bear no direct relationship with the differences found between the theoretical and experimental atomic ratios.

The binding energies for the S $2p$ and Sn $3d_{5/2}$ peaks, and the value of the Sn modified Auger parameter (α^*) (viz. the sum of the binding energy and the kinetic energy of the corresponding Auger transition, Sn_{MNN} for tin) are given in Table 4. The Auger parameter is free from calibration errors in the XPS spectra (choice of binding energy scale) and is more sensitive to the chemical state than are XPS shifts [11].

Fig. 2 shows the S $2p$ emission peak normalized with respect to the Sn $3d_{5/2}$ height. As expected, the signal intensity increases in the sequence $SnS < Sn_2S_3 < SnS_2$, even though, as noted earlier, the ratio to SnS (viz. 1.32 for Sn_2S_3 and 1.86 for SnS_2) is slightly lower than the values derived from stoichiometry considerations. The S $2p$ emission is rather symmetric, taking into account that the $2p_{1/2,5/2}$ doublet is unresolved. So the sulfur must be in a single chemical state, as confirmed by the similarity in the Auger parameter and FWHM values (see Table 4). This is consistent with the structural properties of these compounds as sulfur occupies equivalent positions in the three systems.

The emission peaks of Sn $3d$ are shown in Fig. 3. A significant, somewhat unexpected finding is the high symmetry of the signal for Sn_2S_3, which is comparable to those for SnS and SnS_2 [12] in spite of the presence of two valence states [Sn (II) and Sn (IV)]. Also, the Sn binding energy for Sn_2S_3 is not intermediate between

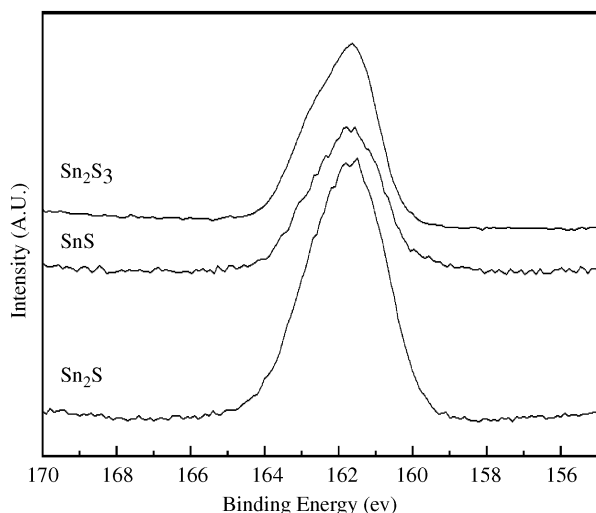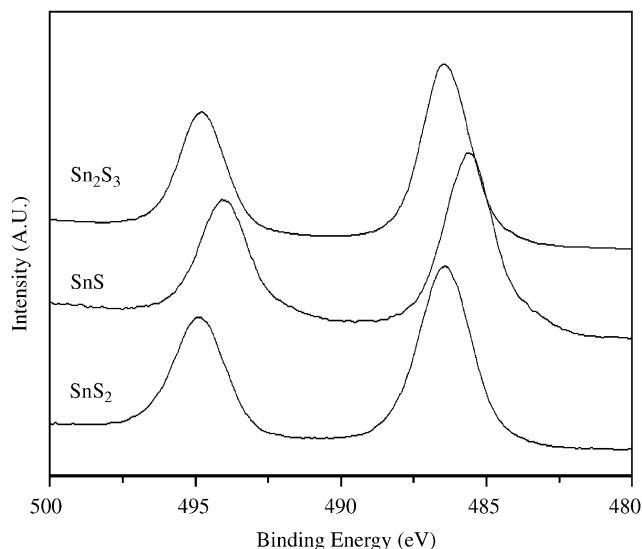Fig. 2. S $2p$ emission peaks for (a) SnS, (b) SnS_2 and (c) Sn_2S_3.

Fig. 3. Sn $3d$ emission peaks for (a) SnS, (b) SnS_2 and (c) Sn_2S_3.

Table 5
Bond distances (in nm) for $Sn_2S_3^{16}$

Bondtype	Distance
Sn(II)–S(3)	0.2657 (2×)
Sn(II)–S(2)	0.2797
Sn(II)–S(1)	0.3084
Sn(II)–S(2)	0.3360 (2×)
Sn(II)–S(3)	0.3663 (2×)
Sn(IV)–S(3)	0.2503
Sn(IV)–S(2)	0.2543 (2×)
Sn(IV)–S(1)[a]	0.2581
Sn(IV)–S(1)[b]	0.2657 (2×)

[a] Within the xz plane.
[b] Above and below the xz plane.

those of SnS and SnS_2, as one would expect from the fact that the difference in BE between SnS and SnS_2 (ca. 0.5 eV) is significant and falls outside the experimental error range. In fact, the calculated value, 486.6 eV, is closer to that of SnS_2. Although these results seem to differ from those reported by La Rocque et al. [13], the BE values for SnS and SnS_2 can be reconciled by taking into account the different scales used for calibration. Thus, in Ref. [13], the BE scale was calibrated from the C $1s$ level of adventitious C taken at 285.0 eV. With this reference, the S $2p$ emission extends over 160.7 to 162.1. In our case, this method was unfeasible because the highly clean surface of the samples (particularly SnS and SnS_2) resulted in the C signal being barely detectable. For this reason, we opted for choosing the S $2p_{3/2}$ level

as reference as S^{2-} ion was present in the three samples. Regarding Sn_2S_3, although the Sn $3d_{5/2}$ peak in Ref. [13] was rather symmetric—similarly to those for SnS and SnS_2—, it was resolved into three components. In our opinion, this mathematical artefact is questionable. In fact, the peak calculated for the oxidation found in Sn_2S_3 at 488.2 eV shifted to 487.1 eV for the SnS sample. Moreover, a component at ca. 163.2 eV was calculated for the S $2p_{3/2}$ emission and interpreted as oxygen-bound sulfur. However, this value corresponds to no well-known S–O species such as sulfites or sulfates [14]. Nevertheless, the increased broadening of the Sn $3d_{5/2}$ line observed for Sn_2S_3 relative to SnS and SnS_2 was also found in our samples.

Similar conclusions can be drawn from the Auger parameter, α_{Sn}^*, which shifts from 921.5 in SnS to 920.7 eV in SnS_2. The α_{Sn}^* value calculated for Sn_2S_3 is virtually coincident with that for SnS_2 (see Table 4). However, two subtle differences are worthnoting. First, the FWHM value of the Sn $3d_{5/2}$ of Sn_2S_3, 2.22 eV, is somewhat greater than that found for single-valence compounds. This may reflect a more heterogeneous chemical environment for Sn owing to both the differential coordination number of Sn (IV) and Sn (II), and the variety of Sn–S distances (Table 5) that describe the crystal structure of Sn_2S_3. The second difference concerns plasmon losses, also detected in the XPS experiments. They appear on the lower kinetic side of the photoemission peak and are generated by the transport of electrons coming from a given element through the solid. Accordingly, their intensity or shape depends on the electron occupancy of the conduction band in the substrate [15]. Fig. 4 includes the plasmon structure of the Sn $3d$ spectra for the three compounds. Two peaks are clearly distinguished for SnS and SnS_2 crystals, the energy loss being somewhat greater for the latter compound (the distance from the first plasmon peak—the strongest—to the $Sn_{3/2}$ signal is ca. 20.5 eV for SnS_2 and ca. 16.5 eV for SnS). The main feature of the plasmon peaks for Sn_2S_3 is an intensity decrease with a slight tendency of the energy loss to approach
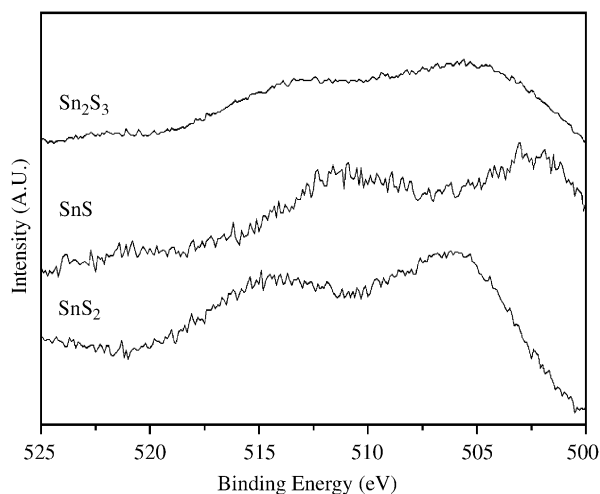
Fig. 4. Sn 3d plasmon loss peaks for (a) SnS, (b) SnS_2 and (c) Sn_2S_3.

Fig. 5. ^{119}Sn NMR spectra for (a) SnS, (b) SnS_2 and (c) Sn_2S_3.

that of SnS. A tentative explanation for the origin of this intensity decrease is that Sn_2S_3 (band gap 0.85 eV) possesses better conducting properties than SnS (band gap 1.3 eV) and SnS_2 (band gap 2.17 eV). Destructuring of plasmon peaks was previously observed in a sample of SnS_2 dosed with Na [7]. It was suggested that Na intercalated into SnS_2 and promoted a semiconducting–metallic transition as a result of the transfer of an electron from the Na atoms to the host network. In any case, the differences between the XPS spectra of Sn_2S_3 and SnS_2 is minimal, so it is difficult to ascertain whether Sn is in a mixed valence state with this spectroscopic technique. The electronic structure of Sn_2S_3 has been examined by Terpstra [16] using ab initio band structure calculations. He found appreciable differences in the 5s and 5p states of Sn (II) and Sn (IV) compared with those of SnS and SnS_2. In fact, the band gap of Sn_2S_3, 0.85 eV, significantly differs from that of SnS and SnS_2. Moreover, it is known the difficulty in the measurement of the chemical shift by XPS for poor conducting samples because the problems of charging of samples add difficulty of defining a reference level from which the binding energy can be measured. The combination of all these factors makes difficult the resolution of the two oxidation states in the mixed valence compound by XPS, taking also into account the proximity in the BE of these oxidation states (see Table 4).

The ^{119}Sn MAS NMR spectra for SnS, Sn_2S_3 and SnS_2 are shown in Fig. 5 and the calculated parameters in Table 6. The spectra for SnS and SnS_2 are consistent with those reported by Mundus et al. [17] and Pietrass et al. [18]. In the case of SnS (space group Pnma), the experimental envelope of the signal centered at −299 ppm spreads over an important spectral region. The non-axial symmetry inferred ($\eta = 0.4$) describes the highly distorted octahedral environment of tin atoms
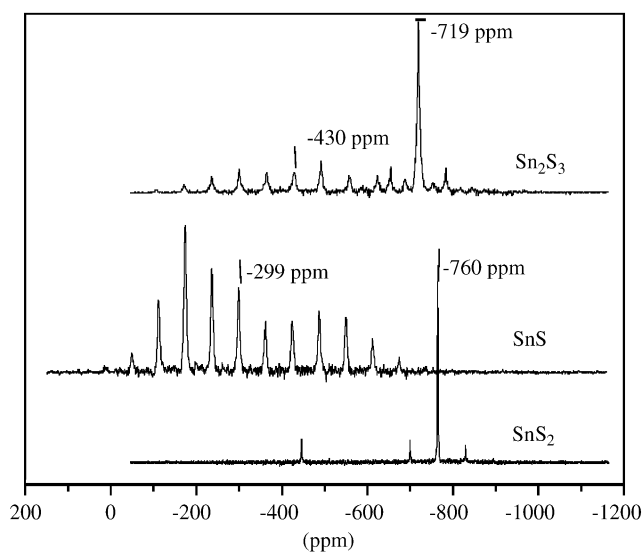
Table 6
Chemical shifts, anisotropy and skew parameters obtained from the spectral analysis of various tin sulfides

Compound	δ (ppm)	$\Delta\sigma$ (ppm)	η (ppm)
SnS	−299 (5.4)[a]	−370	0.4
Sn_2S_3	−430 (7.0)	−390	0.7
	−719 (4.8)	<50	—
SnS_2	−760 (0.4)	—	—

[a] Values in parenthesis: full-widths at half-maximum.

[19] and is somewhat lower than that reported by Mundus et al. [17]. Four S atoms are located in the plane of the sulfide layer, at distances of 0.2665(2) and 0.3290(2) nm. A fifth S atom normal to this plane is present at a distance of 0.2627 nm. Tin coordination is completed by a weak bond to an S atom belonging to a neighboring double layer, at a distance of 0.3388 nm. As a consequence of octahedral distortions, the chemical shift anisotropy ($\Delta\sigma$) of this signal is −370 ppm. By contrast, the tin atoms in SnS_2 (space group P3m1) are coordinated by a regular octahedron of sulfur atoms with bond distances of 0.2571 nm [20]. In this case, chemical shift anisotropies of the signal centered at −760 ppm cannot be determined accurately. In any case, the calculated value for the chemical shift anisotropy, $\Delta\sigma \approx -50$ ppm, is comparable with that reported in Ref. [18]. At present, we have no satisfactory explanation for the small, narrow additional line observed for SnS_2 at about −450 ppm. It might be ascribed to the presence of a secondary amorphous phase not detected by the XRD technique. Taking into account the absence of iodine in XPS spectra of this sample, this signal must correspond to Sn atoms

coordinated either to sulfur or, less likely, oxygen atoms. The above results reflect differences in electron distribution around tin atoms in Sn^{2+} and Sn^{4+} electron configurations, particularly as regards the stereochemical activity of the $5s^2$ lone pair in Sn^{2+}.

The spectrum for Sn_2S_3 has two resonances centered at -430.0 and -719.1 ppm that have also been assigned to Sn(II) and Sn(IV), respectively. The absence of peaks corresponding to SnS and SnS_2 is indicative of the single-phase character (high purity) of the studied samples. In Sn_2S_3, tin atoms [Sn(II) and Sn(IV)] and three sulfur atoms [S(1), S(2) and S(3)] occupy five different $4c$ positions in the orthorhombic space group *Pnma* (see Table 2). The Sn–S bond distances are given in Table 5. The Sn(IV)-S_6 octahedron is only weakly distorted, with bond distances ranging from 0.2495 to 0.2609 nm. Small differences in Sn–S distances or S–Sn–S angles could be the origin of the observed differences in chemical shift values for the octahedral components of SnS_2 and Sn_2S_3 sulfides. In which concerns the Sn (II) signal, isotropic chemical shift values measured in Sn_2S_3 and SnS differ considerably (-430 and -199 ppm, respectively), indicating that important changes are produced in the Sn (II) coordination of the two compounds. In the sulfides studied in this work, the observed decrease in chemical sift of the Sn(II) signals, from -299 to -430 ppm, can be ascribed to the increase in coordination number from 6 in SnS to 8 in Sn_2S_3. Similar results have been reported in the Na–Sn^{IV}–S system, where the measured chemical shifts decreased for $Sn^{IV}S_4$, $Sn^{IV}S_5$, $Sn^{IV}S_6$ coordinations [17]. In Sn_2S_3, three S atoms are at a shorter distance and the other five at a longer one (see Table 5). From this fact, severe distortions detected in the bicapped trigonal prism are responsible for important chemical shift anisotropies detected in the Sn(II) signal of Sn_2S_3 ($\Delta\sigma = -390$ ppm and $\eta = 0.7$). In the case of SnS, strong distortions in the octahedral coordination of Sn(II) produced important chemical shift anisotropies ($\Delta\sigma = -370$ ppm and $\eta = 0.4$). Finally, the signal broadening of the mixed valence compound is also indicative of higher heterogeneity in the coordination of tin atoms relative to the single-valence compounds.

The ability of ^{119}Sn NMR to unambiguously differentiate the two oxidation states of tin arises from the detection time of this resonance technique (time scale $\approx 10^{-8}$ s), which is shorter than the lifetimes of the valence states. Other resonance techniques such as ^{119}Sn Mösbauer spectrometry also allow Sn(II) and Sn(IV) to be distinguished [21]. However, NMR spectra provide a clearer description of the tin environment since the resolution of two valence states was higher. In Mössbauer spectroscopy, the isomer shift values for Sn(IV) in Sn_2S_3 and SnS_2 are similar (1.03–1.16 mm/s) [21,22] and the distortion of the [$Sn^{IV}S_6$] octahedra in $Sn_2S_3$is hardly detected [21]. By contrast, significative

differences are detected in the chemical shifts values of octahedra in ^{119}Sn NMR MAS spectra of the two compounds (see Table 6). In which concerns the Sn (II) signal, the isomer shift value measured in Sn_2S_3 (3.52–3.50 mm/s, [20,21]) is somewhat larger than that found in SnS, for which values of 3.23–3.31 mm/s have been reported [22,23]. Moreover, the quadrupole splitting for Sn (II) in Sn_2S_3 (0.95–0.99 mm/s) is somewhat larger than that found in SnS (0.85–0.87 mm/s). Chemical shift anisotropies deduced from ^{119}Sn NMR spectra of Sn (II) in SnS and Sn_2S_3 are given in Table 6. In all cases, differences on isotropic chemical shifts, chemical shift anisotropies and asymmetry parameters are larger than those found in Mössbauer spectroscopy.

4. Conclusions

Sn_2S_3 is the only mixed valence compound in the Sn–S system that could be synthesized using chemical vapor transport methods with iodine as carrier agent. The XPS and ^{119}Sn NMR techniques were used to distinguish the two valence states present in Sn_2S_3. The high symmetry of the Sn $3d$ emission peak and its binding energy (similar to that of SnS_2) prevents the use of XPS as a fingerprint technique for mixed valence tin sulfides. On the other hand, the ^{119}Sn NMR spectrum for Sn_2S_3 exhibits two resonances that can be assigned to Sn(II) and Sn(IV). Moreover, the chemical shifts of these signals are rather different from those of the single-valence compounds (SnS and SnS_2), which is consistent with the differences in coordination and/or the Sn–S bond distances. The NMR technique is the most suitable choice for identifying Sn−S mixed valence compounds owing to its ability to detect the finest details of the Sn environment.

References

[1] D. Mootz, H. Puhl, Acta Crystallogr. 23 (1967) 471.
[2] L.D.C. Bok, J.C.A. Boeyens, J.S. Afr. Chem. Inst. 10 (1957) 49;
    W. Albers, K. Schol, Philips Res. Rep. 16 (1961) 329.
[3] H. Liu, L.L.Y. Chang, J. Alloys Compds. 185 (1992) 183.
[4] R. Kniep, D. Mootz, U. Severin, H. Wunderlich, Acta. Crystallogr. B 52 (1982) 2022.
[5] JCPDS-ICDD 14–538; 27–900.
[6] L.S. Price, I.P. Parkin, A.M.E. Hardy, R.J.H. Clark, Chem. Mater. 11 (1999) 1792.
[7] L. Hernán, J. Morales, L. Sánchez, J. Santos, J. Electrochem. Soc. 146 (1999) 657;
    J.P. Espinós, A.R. González-Elipe, L. Hernán, J. Morales, L. Sánchez, J. Santos, Surf. Sci. 426 (1999) 259;

J. Morales, J. Santos, J.R. Ramos Barrado, J.P. Espinós, A.R. González-Elipe, J. Solid State Chem. 150 (2000) 391;
L. Hernán, J. Morales, L. Sánchez, J. Santos, J.P. Espinós, A.R. González-Elipe, J.P. Holgado, Surf. Sci. 477 (2001) L295.

[8] L. Hernán, J. Morales, L. Sánchez, J.L. Tirado, J.P. Espinós, A.R. González-Elipe, Chem. Mater. 7 (1995) 1576.

[9] H.M. Rietveld, J. Appl. Crystallogr. 2 (1969) 65.

[10] A.C. Larson, R.B. von Dreele, Los Alamos National Laboratory Report No. LA-UR-856-748, 1994.

[11] C.D. Wagner, Faraday Discuss. Chem. Soc. 60 (1975) 291.

[12] P. Baláz, T. Ohtani, Z. Bastl, E. Boldizárová, J. Solid State Chem. 144 (1999) 1;
Q. Yang, K. Tang, D. Zhang, Y. Qian, J. Solid State Chem. 164 (2002) 106.

[13] A.G. LaRocque, E. Belin-Ferré, M.F. Fontaine, C. Senemaud, J. Olivier-Fourcade, J.C. Jumas, Philos. Mag. B 80 (2000) 1933.

[14] C.D. Wagner, W.M. Riggs, L.E. Davis, J.F. Moulder, G.E. Mullenberg, Handbook of X-ray Photoelectron Spectroscopy, Perkin–Elmer Corporation, Physical Electronics Division, Eden Pairie, MN, 1979.

[15] B.D. Ratner, D.G. Castner, in: J.C. Vickerman (Ed.), Surface Analysis, Wiley, New York, 1997, p. 71.

[16] H.J. Terpstra, Ph.D. Dissertation, University of Groningen, 1967.

[17] C. Mundus, G. Taillades, A. Pradel, M. Ribes, Solid State Nucl. Magn. Reson. 7 (1996) 141.

[18] T. Pietrass, F. Taulelle, P. Lavela, J. Olivier-Fourcade, J.C. Jumas, S. Steuernagel, J. Phys. Chem. B 101 (1997) 6715.

[19] H. Wiedemeier, H.G. von Schnering, Z. Kristallogr. 148 (1978) 295.

[20] R.M. Hazen, R.M. Finger, Am. Miner. 63 (1978) 289.

[21] C. Adenis, J. Olivier-Fourcade, J.C. Dumas, E. Philippot, Rev. Chim. Miner. 23 (1986) 735.

[22] G. Amthauer, J. Fenner, S. Hafner, W.B. Holzapfel, R. Keller, J. Chem. Phys. 70 (1979) 4837.

[23] J.C. Jumas, S. del Bucchia, E. Philippot, M. Maurin, J. Solid State Chem. 41 (1988) 50.